JACS
JOURNAL OF THE AMERICAN CHEMICAL SOCIETY
Article
pubs.acs.org/JACS

Understanding the Quenching Effects of Aromatic C−H- and C−D-Oscillators in Near-IR Lanthanoid Luminescence

Christine Doffek,[†] Nicola Alzakhem,[†] Caroline Bischof,[†] Jessica Wahsner,[†] Tuba Güden-Silber,[†] Joachim Lügger,[†] Carlos Platas-Iglesias,*[,‡] and Michael Seitz*[,†]

[†]Inorganic Chemistry I, Department of Chemistry and Biochemistry, Ruhr-University Bochum, 44780 Bochum, Germany
[‡]Departamento de Química Fundamental, Universidade da Coruña, Campus da Zapateira-Rúa da Fraga 10, 15008 A Coruña, Spain

Supporting Information

ABSTRACT: Several series of selectively deuterated 2,2′-bipyridine-based cryptates with the near-IR emissive lanthanoids Pr, Nd, Er, and Yb are reported. The structural and luminescence properties of these complexes have been comprehensively investigated. A combination of experimental techniques (X-ray crystallography, lanthanoid-induced NMR shift analysis, luminescence, vibrational near-IR absorption) and theoretical concepts has been applied with a focus on nonradiative deactivation through multiphonon relaxation of lanthanoid excited states by aromatic, high-energy C−(H/D) oscillators. It is shown that the characteristics for the overtones of these vibrational modes deviate substantially from harmonic oscillators and that anharmonicity within a local-mode Morse model is an essential parameter for any accurate description. The spectral overlap integrals (SOIs) of lanthanoid electronic states with aromatic C−(H/D) overtones are evaluated quantitatively for different lanthanoid/oscillator combinations and the implications for luminescence enhancement through deuteration is discussed. Simple Gaussian functions are proposed as appropriate mathematical forms for the empirical approximation of SOIs.

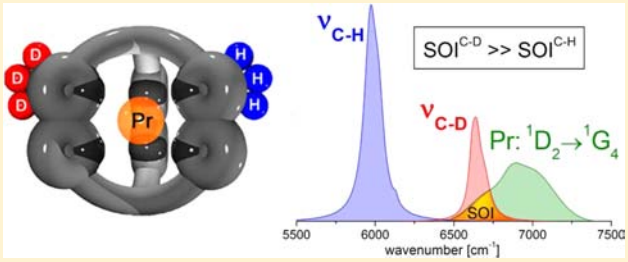

1. INTRODUCTION

Nonradiative deactivation of excited states in molecular compounds by the interaction of electronic and vibrational levels is one of the most fundamental phenomena in the photophysics of luminescent systems. In general, this phenomenon is highly complex and dependent on a myriad of different parameters, which makes the analysis and the theoretical description of these processes very difficult. Consequently, a general knowledge of the intricacies determining nonradiative deactivation is still in its infancy despite of its importance for almost all fields of theoretical and applied photophysics. One of the few cornerstones for the description of nonradiative decay is the so-called "energy gap law" (EGL),[1] which in its simplest version predicts the rate of nonradiative deactivation k_{nr} to be

$$k_{nr} = C_1\, e^{-[C_2(\Delta E/\hbar\omega_M)]} \quad (1)$$

where C_1 and C_2 are empirically fitted parameters characteristic for a particular system, ΔE is the energy gap between the initially populated state of interest and the next lower state, and ω_M is the frequency of a deactivating vibrational mode. The derivations of the EGL and its various refined versions assume the presence of harmonic oscillators. In addition, constraints are often made concerning relative energies in the system (e.g., $\Delta E \gg \hbar\omega_M$ or $\hbar\omega_M \gg k_BT$). In the field of inorganic photophysics, the EGL has been shown to work well for a number of important cases, including luminescent lanthanoid ions in solid host matrices[2] and the decay of certain charge-transfer excited states in transition metal polypyridine complexes.[3] The often encountered application of the EGL to the near-IR luminescence of molecular lanthanoid complexes,[4] however, is problematic, because the assumptions underlying the EGL are not valid, that is, nonradiative decay is predominantly mediated by the most anharmonic oscillators X−H (with X = O, N, C) and the energy gap ΔE is usually within one to three multiples of the accepting vibrational mode. For this situation, a different model was proposed by Ermolaev and Sveshnikova which is called the "inductive-resonant mechanism of non-radiative transitions".[5] Within this approach, the energy transfer from the lanthanoid to the anharmonic X−H oscillators is considered to primarily occur via electric dipole−dipole interactions under inductive-resonant conditions. This model is completely analogous to the well-known Förster resonance energy transfer (FRET) for organic fluorophores.[6] In this picture, the electronic state at the lanthanoid is the donor for the resonance energy transfer (RET) and a matching vibrational state is the RET acceptor. Under the conditions of the inductive-resonant theory, k_{nr} due to Förster energy transfer from the lanthanoid excited state to the oscillator can be expressed by eq 2:[5]

Received: August 1, 2012
Published: September 25, 2012

   dx.doi.org/10.1021/ja307339f | J. Am. Chem. Soc. 2012, 134, 16413−16423

$$k_{nr} = \frac{9000\ln(10)\cdot k_r\cdot\kappa^2}{128\cdot\pi^2\cdot n^4\cdot N_A\cdot r^6}\cdot SOI \quad (2)$$

In eq 2, k_r is the rate of the radiative transition in the absence of any nonradiative deactivation processes, κ is a factor depending on the relative orientations of the transition dipole moments of the donor (the lanthanoid) and the acceptor moiety (e.g., a X−H oscillator), n is the refractive index of the medium, N_A is Avogadro's number, and r is the distance between the lanthanoid and the oscillator. SOI is a Förster-type spectral overlap integral of the form

$$SOI = \int I_{norm}(\tilde{\nu})\cdot\varepsilon_{vib}(\tilde{\nu})\cdot\tilde{\nu}^{-4}\,d\tilde{\nu} \quad (3)$$

The integrand of SOI contains several parameters as functions of the wavenumber $\tilde{\nu}$. $I_{norm}(\tilde{\nu})$ is the emission spectrum normalized to unit area and $\varepsilon_{vib}(\tilde{\nu})$ is the decimal molar vibrational absorption coefficient. In general, the calculation of nonradiative deactivation rates k_{nr} using eq 2 requires a plethora of specific information that is often not easy to come by. Accurate data on the very fundamental parameters k_r, r, and $\varepsilon_{vib}(\tilde{\nu})$ in solution are experimentally rather tedious to obtain. The determination of the vibrational absorption spectrum $\varepsilon_{vib}(\tilde{\nu})$ of X−H oscillators in solvent molecules (e.g., in H_2O) in the first, second, and outer solvation sphere is often especially difficult or even impossible. First, because the exact geometric relationship is usually not known and second, because the absorption spectrum of the bulk solvent (which is often easily accessible) may not reflect the vibrational properties of oscillators most relevant for quenching, for example, a water molecule directly bound to the lanthanoid center. $\varepsilon_{vib}(\tilde{\nu})$ of the latter entities is extremely hard to quantify because it usually constitutes only a tiny fraction in the presence of a huge excess of bulk solvent molecules. The mathematical structure of the SOI is also tedious from a theoretical viewpoint. The integral neither has a general analytical solution nor a convenient series expansion, even with various approximations. Taken together, the evaluation of nonradiative deactivation rates k_{nr} according to eq 2 is an arduous task because it necessitates the determination of many, experimentally rather inaccessible parameters for every individual case. It would therefore be highly desirable to simplify some aspects of this procedure, for example, by empirical parametrization of certain factors in eq 2, in order to arrive at a more convenient model for molecular complexes in solution.

Apart from the extensive investigations by Ermolaev and Sveshnikova themselves,[5] there have been a number of efforts over the years to formalize systematic trends in nonradiative deactivation for molecular lanthanoid complexes on the basis of empirical data.[5] Selected examples include the work of Horrocks[7] and Parker,[8] who have very successfully developed empirical methods to determine the number of inner-sphere water molecules based on the comparison of luminescence quenching rate differences in H_2O and D_2O solutions, or the studies by Quochi[9] and Monguzzi,[10] who have tried to rationalize the nature and the effects of C−H oscillators on nonradiative deactivation in luminescent erbium complexes. Overall, however, very few systematic investigations in this field have been published.

We have recently initiated our own investigations in this direction.[11] Our approach is characterized by the synthesis of tailor-made, selectively deuterated lanthanoid complexes that allows us to address very specific questions regarding nonradiative deactivation of near-IR emitting lanthanoids by C−H and C−D oscillators. The complexes [**D**$_x$]-**Ln** (Figure 1)

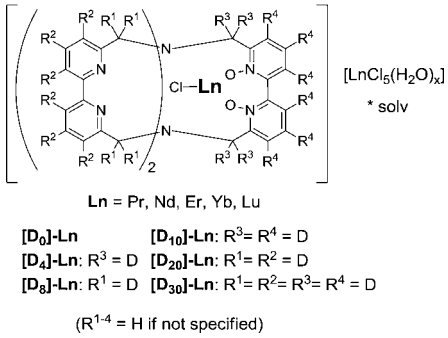

Figure 1. Synthesized lanthanoid cryptates [**D**$_x$]-**Ln**.

that we use for this purpose are based on the seminal work by Jean-Marie Lehn on 2,2′-bipyridine-based cryptands.[12] [**D**$_x$]-**Ln** features a tris(bipyridine) cryptand where one arm is modified with a *N*,*N*′-dioxide motif. The latter structural element, combined with the tight binding of an external chloride anion in methanolic solution, imparts great rigidity to the resulting lanthanoid cryptates.[11b] The isotopologic cryptates [**D**$_x$]-**Ln** are an ideal model system for a number of reasons: (1) They are highly stable in solution and show luminescence with many near-IR emitting lanthanoids (here: Pr, Nd, Er, Yb). (2) Due to the rigid cryptate structure, the position of all C−(H/D) oscillators are fixed and the exact geometry can be determined in solution by lanthanoid-induced NMR shift analysis. (3) The different isotopologic cryptates have the same structure and should have similar sensitization pathways and efficiencies. This makes the comparison of nonradiative deactivation rates according to eq 2 much easier, because certain parameters can be assumed to stay constant for isotopologic oscillators (e.g., k_r, κ, r). (4) The cryptates [**D**$_x$]-**Ln** contain aromatic C−(H/D) units, that can often be modeled as Morse oscillators, which promises to make the empirical and theoretical description of their behavior rather simple.

In this report, we detail the photophysical characterization of these isotopologic cryptates [**D**$_x$]-**Ln** in the framework of the inductive-resonant model for nonradiative deactivation. We determine the solution structures of the complexes and validate these cryptates as an ideal model system that is isostructural across the lanthanoid series. Most importantly, we show the nature and impact of the differences in the vibrational anharmonicities of the aromatic C−(H/D) oscillators and, on the basis of the obtained empirical measurements, propose a new approximation for the critically important parameter SOI with a very simple mathematical structure.

2. RESULTS

2.1. Synthesis. The lanthanoid cryptates were synthesized in analogy to the sequence previously reported for the corresponding europium cryptate [**D$_0$**]-**Eu**[12] and the perdeuterated cryptates [**D$_{30}$**]-**Ln**[11b] (see the Supporting Information). In contrast to previous reports,[12,11b] the bulk material consists of a 1:1 mixture of the expected lanthanoid cryptates and a "free" lanthanoid complex $[LnCl_5(H_2O)]^{2-}$. The somewhat surprising presence of the latter species in the bulk materials is supported by elemental analyses and by crystal structures[13] of [**D$_0$**]-**Er** and [**D$_0$**]-**Yb** (see the Supporting

dx.doi.org/10.1021/ja307339f | J. Am. Chem. Soc. 2012, 134, 16413−16423

Information). The species $[LnCl_5(H_2O)]^{2-}$ neither contains nonexchangeable protons (cf. ^{1}H NMR and X−H vibrational absorption spectroscopy) nor has an antenna moiety for the sensitization of lanthanoid luminescence. Therefore, the presence of this species does not interfere with measurements on the cryptates in solvents (e.g., CD_3OD in this study) that provide efficient solvent separation between the different complexes (i.e., positively charged cryptate species and negatively charged "free" lanthanoid-chlorido complexes).

2.2. DFT Calculations and Lanthanoid-Induced Paramagnetic ^{1}H NMR Shift Analysis. To gain information on the solution structure of the complexes $[\mathbf{D}_x]$-**Ln**, we performed full geometry optimizations by DFT calculations in MeOH solution. The obtained geometry for $[\mathbf{D}_0]$-**Yb** resembles the corresponding X-ray crystal structure of the cryptate (see Supporting Information), and shows a nearly undistorted C_2 symmetry, where the symmetry axis contains the chloride ligand and the Yb^{III} ion (Figure 2).

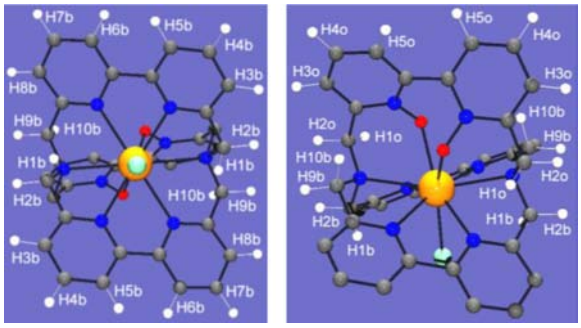

Figure 2. Structure of $[\mathbf{D}_0]$-**Yb** obtained by DFT geometry optimization. Color scheme: H, white; C, gray; N, blue; O, red; Cl, turquoise; Yb, orange.

The bond distances between the lanthanoid and the coordinating donor atoms in the calculated cryptate $[\mathbf{D}_0]$-**Yb** are in very good agreement with the ones found in the crystal structure (see Supporting Information) with an average unsigned deviation of only 1.1%. Geometry optimization of the Pr, Nd and Er cryptates in methanol gave an isostructural series of cryptates $[\mathbf{D}_0]$-**Ln** with lanthanoid-oscillator distances for the aromatic protons as listed in Table 1. The C−H oscillators on the *N*,*N*′-dioxide unit (Table 1: H3o−H5o) are further away from the Ln compared to the C−H moieties on the bpy arms (Table 1: H3b−H8b). The dependence of k_{nr} on the distance r ($k_{nr} \propto r^{-6}$) in eq 2 implies that the vibrational overtones of the *N*,*N*′-dioxide moiety should quench less compared to their bpy counterparts. This geometrical factor g amounts in our case to 1.43−1.53 going from Pr to Yb (Table 1, last row).

The ^{1}H NMR spectra (see the Supporting Information) of the cryptates $[\mathbf{D}_0]$-**Ln** (Ln = Pr, Nd, Er, Yb) recorded in CD_3OD show 15 signals, which points to an effective C_2 symmetry of these species in solution. In the case of the Yb^{III} cryptate, a partial assignment of the spectrum could be achieved by comparing the NMR spectra recorded for the different isotopologic complexes $[\mathbf{D}_x]$-**Yb** (x = 0, 4, 8, 10, and 20). Additionally, the ^{1}H NMR peaks due to the methylenic protons of the ligand (H1o, H2o, H1b, H2b, H9b and H10b) can be grouped into two different sets according to their relative line broadening: three resonances with Lorentzian linewidths at half height of 236−501 Hz (at 400 MHz and 298 K), and three signals with line widths in the range of 90−188 Hz. These two sets of signals correspond to two sets of Yb^{III}−proton distances, the broader resonances being associated with the protons closer to the metal ion.[14] Thus, the broader signals were assigned to protons closer to Yb, while the second set of signals was assigned to ones further away from the metal center. A full assignment of the spectrum was performed by exploiting the structural information encoded in the paramagnetic shifts (see below) and the constraints obtained from line width analysis. This procedure has some circular reasoning, as it assumes a given structure of the complex in solution for spectral assignment. However, it has been shown that in this procedure both the assignments and the solution structure are acceptable if a good fit between experimental and calculated data is obtained.[15] For a given nucleus i, the isotropic paramagnetic shift δ_{ij}^{para} induced by a lanthanoid ion j is generally a combination of the Fermi contact (δ_{ij}^{con}) and dipolar (δ_{ij}^{dip}) contributions:[15]

$$\delta_{ij}^{para} = \delta_{ij}^{exp} - \delta_i^{dia} = \delta_{ij}^{con} + \delta_{ij}^{dip} \quad (4)$$

where the diamagnetic contribution δ_i^{dia} is obtained by measuring the chemical shifts for analogous diamagnetic complexes. In the present case, the ^{1}H NMR shifts observed for the Lu^{III} cryptate were used to estimate the diamagnetic contribution. However, some pairs of the proton signals of $[\mathbf{D}_0]$-**Lu** could not be assigned due to the limited amount of sample available for recording 2D HSQC and HMBC spectra (H3b−H8b, H4b−H7b and H5b−H6b). Thus, for these pairs of proton nuclei the diamagnetic contribution was estimated from the corresponding averaged value. The hyperfine ^{1}H NMR shifts in Yb^{III} complexes are considered to be largely pseudocontact in origin, and we therefore performed the analysis of the paramagnetic shifts observed in the ^{1}H NMR spectrum of $[\mathbf{D}_0]$-**Yb** with the assumption that they are dominated by dipolar contributions, which can be written as linear combinations of the five components of the susceptibility tensor χ as given by the following:[16]

Table 1. Average Distances r(Ln−H) for Aromatic Protons Calculated by DFT in Methanolic Solution for the Paramagnetic Lanthanoid Cryptates $[\mathbf{D}_0]$-Ln (Ln = Pr, Nd, Er, Yb)[a]

	r(Pr−H) [Å]	r(Nd−H) [Å]	r(Er−H) [Å]	r(Yb−H) [Å]
H3o	5.924(2)	5.925(3)	5.896(3)	5.892(0)
H4o	6.918(2)	6.920(2)	6.901(2)	6.904(1)
H5o	6.197(1)	6.197(1)	6.156(2)	6.157(0)
H3b	5.652(5)	5.647(4)	5.539(2)	5.526(0)
H4b	6.542(2)	6.536(1)	6.420(1)	6.402(0)
H5b	5.743(2)	5.737(2)	5.637(2)	5.620(0)
H6b	5.708(3)	5.703(3)	5.661(1)	5.644(0)
H7b	6.528(2)	6.524(3)	6.503(1)	6.483(0)
H8b	5.678(3)	5.674(3)	5.646(1)	5.626(0)
$g = \frac{2\cdot\sum_{bpyO2}(r_i)^{-6}}{\sum_{bpy}(r_i)^{-6}}$	1.43	1.44	1.50	1.53

[a]Averaged over the two symmetry-related H-positions, absolute deviation given in parentheses.

dx.doi.org/10.1021/ja307339f | J. Am. Chem. Soc. 2012, 134, 16413−16423

$$\delta_{ij}^{dip} = \left(\chi_{zz} - \frac{1}{3}Tr\chi\right)\left(\frac{3z^2 - r^2}{r^5}\right) + (\chi_{xx} - \chi_{yy})\left(\frac{x^2 - y^2}{r^5}\right) + \chi_{xy}\left(\frac{4xy}{r^5}\right) + \chi_{xz}\left(\frac{4xz}{r^5}\right) + \chi_{yz}\left(\frac{4yz}{r^5}\right) \quad (5)$$

$$\text{with} \quad r = \sqrt{x^2 + y^2 + z^2} \quad (6)$$

In eq 5, the Cartesian coordinates of atom i relative to the location of a paramagnetic ion are used in place of the more usual spherical coordinates. In the principal magnetic axis system, χ_{xy}, χ_{xz} and $\chi_{yz} = 0$, and for axial symmetry, $\chi_{xx} - \chi_{yy} = 0$. According to the Neumann's principle,[17] one of the principal magnetic axis of [**D$_0$**]-**Yb** must coincide with the 2-fold symmetry axis of the molecule. Thus, we assumed that the z axis of the magnetic susceptibility tensor coincides with the C_2 axis of the molecule. As a consequence, we considered only three (rather than five) parameters in the analysis of the paramagnetic shifts, namely, the axial $[\chi_{zz} - 1/3(\chi_{xx} + \chi_{yy} + \chi_{zz})]$ and rhombic $(\chi_{xx} - \chi_{yy})$ anisotropies of the magnetic susceptibility tensor χ, and the orientation of the magnetic axis in the xy plane given by an angle α.[18] The DFT structure of the [**D$_0$**]-**Yb** complex provides a very good agreement between the experimental and calculated Yb^{III}-induced shifts with an agreement factor AF$_j$ = 0.018. The excellent agreement observed between the experimental and calculated Yb^{III}-induced paramagnetic shifts unambiguously proves that our DFT calculations provide a very accurate description of the structure of the [**D$_0$**]-**Yb** complex (Figure 3). Indeed, poorer

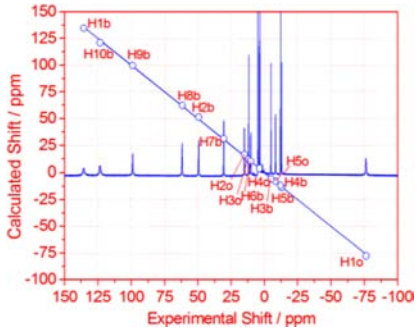

Figure 3. ^{1}H NMR (400 MHz, 298 K) spectrum of [**D$_0$**]-**Yb** recorded in CD_3OD solution and plot of experimental shifts versus those calculated with eq 5 and the DFT geometry. The solid line represents a perfect fit between experimental and calculated values.

agreement factors (AF$_j \approx$ 0.06–0.09) have been previously obtained, and considered to be acceptable, for different nonaxial Yb^{III} complexes.[19] As expected for a nonaxial system, the calculated $\chi_{zz} - 1/3(\chi_{xx} + \chi_{yy} + \chi_{zz})$ and $\chi_{xx} - \chi_{yy}$ values define a rhombic magnetic susceptibility tensor. Among the other paramagnetic Ln^{III} ions investigated in this study, Pr^{III} possesses the lowest theoretical ratio of the contact and dipolar contribution (0.268, 1.06, and 0.466 for Pr, Nd, and Er, respectively), which is however considerably higher than for Yb^{III} (0.118). Thus, we also analyzed the Pr^{III}-induced paramagnetic shifts with eq 5 and the DFT geometry of the complex. The assignment of the proton signals followed the same approach described for the Yb^{III} cryptate (see the Supporting Information).

The agreement is somewhat poorer for the Pr^{III} cryptate in comparison to the Yb^{III} analogue, which suggests that contact contributions might not be negligible for certain nuclei, particularly those experiencing small paramagnetic shifts such as the protons H2o or H3o. The reasonably good agreement observed between the experimental and calculated shifts again demonstrates that our DFT calculations provide a good model for the structure in solution. The analysis for Nd and Er was not possible due to the large contact contributions, but it is very likely that they resemble the corresponding Pr and Yb complexes due to the very similar ionic radii (Pr/Nd and Er/Yb). This is also supported by the cryptate models obtained from the DFT calculations.

2.3. Luminescence Spectroscopy. Steady-state emission spectra of [**D$_x$**]-**Ln** (Ln = Pr, Nd, Er, Yb) in CD_3OD show strong near-IR luminescence with the characteristic bands for the lanthanoids Yb, Nd, Er, and Pr (Figure 4). To see whether

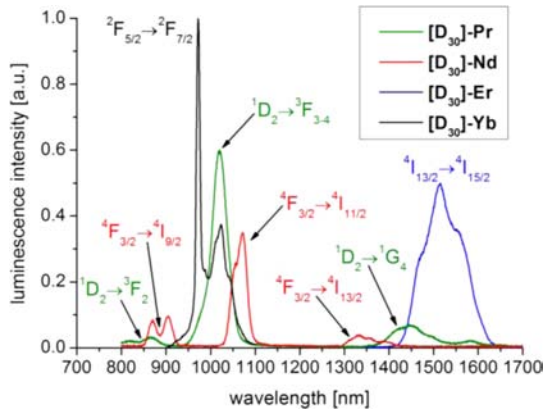

Figure 4. Steady-state emission spectra of [**D$_{30}$**]-**Ln** (Ln = Yb, Nd, Er, Pr) in CD_3OD (λ_{exc} = 304 nm).

the different deuteration patterns influence the sensitization process, we measured low temperature emission spectra of the isotopologic complexes [**D$_x$**]-**Lu** (x = 0, 4, 8, 10, 20, 30). In all cases, we obtained almost identical phosporescence bands around λ_{max} = 531 nm (see the Supporting Information), which seems to be an indication that deuteration does not substantially alter sensitization (e.g., by potentially shifting the energy of the triplet level).

Luminescence lifetime measurements in CD_3OD gave monoexponential decay kinetics for all cryptates [**D$_x$**]-**Ln** (Ln = Nd, Er, Yb) (Table 2). The lifetimes for the praseodymium cryptates were too short (τ_{obs} < ca. 0.8 μs) to be measurable with our instrumental setup. Global fitting of the lifetime data gave nonradiative deactivation rate differences (C–H minus C–D) for the different oscillator groups (Table 3).

For some lanthanoids, the lifetime in CH_3OH and CD_3OD can also provide insight into the number q_{MeOH} of methanol molecules that directly bind to the metal center in methanolic solutions. This can be achieved using the empirical equations developed by Beeby et al. for the lanthanoids Yb and Nd.[20] We have previously reported that [**D$_{30}$**]-**Yb** has a q_{MeOH} value of close to zero (q_{MeOH} = −0.08).[11b]

The same holds true for [**D$_{30}$**]-**Nd** with lifetimes of τ_{obs} = 2.89 μs in CD_3OD (Table 2) and τ_{obs} = 0.85 μs in CH_3OH, giving q_{MeOH} = −0.16.[20] The negative values of q_{MeOH} in both cases might be connected to the fact that the perdeuterated cryptates do not contain any C–H oscillators, the impact of which is implicitly assumed and accounted for in the empirical equation used. The fact that q_{MeOH} is essentially zero for both

dx.doi.org/10.1021/ja307339f | J. Am. Chem. Soc. 2012, 134, 16413–16423

Table 2. Luminescence Lifetimes τ_{obs} and Deactivation Rates $k_{obs} = 1/\tau_{obs}$ for $[D_x]$-Ln in CD_3OD (λ_{exc} = 304 nm)[a]

					Nd[b]			Er[c]			Yb[d]		
$[D_x]$-Ln	w[e]	x[e]	y[e]	z[e]	τ_{obs} [μs]	k_{obs}[f] [10^2 ms^{-1}]	calc. k_{obs}[g] [10^2 ms^{-1}]	τ_{obs} [μs]	k_{obs}[f] [10^2 ms^{-1}]	calc. k_{obs}[g] [10^2 ms^{-1}]	τ_{obs} [μs]	k_{obs}[f] [10^2 ms^{-1}]	calc. k_{obs} [10^2 ms^{-1}]
$[D_0]$	0	0	0	0	0.74	13.5(4)	13.4	1.74	5.8(7)	5.7	11.4	88(1)	88
$[D_4]$	1	0	0	0	0.92	10.9(2)	10.9	1.98	5.1(5)	5.1	15.0	67(5)	67
$[D_8]$	0	0	2	0	1.38	7.2(2)	7.2	2.57	3.9(2)	3.9	24.8	40(1)	40
$[D_{10}]$	1	1	0	0	0.94	10.7(5)	10.8	2.09	4.8(3)	4.8	15.7	64(5)	64
$[D_{20}]$	0	0	2	2	1.63	6.1(1)	6.1	3.03	3.3(1)	3.3	29.1	35(3)	35
$[D_{30}]$	1	1	2	2	2.89	3.5(1)	3.5	4.05	2.5(1)	2.5	91.0[h]	11(1)	11

[a]The measured values are averages of at least three independent experiments. [b]λ_{em} = 1065 nm. [c]λ_{em} = 1525 nm. [d]λ_{em} = 975 nm. [e]w = no. of bpy-*N*,*N*′-dioxide arms deuterated in benzylic position, x = no. of bpy-*N*,*N*′-dioxide arms deuterated in aromatic position, y = no. of bpy arms deuterated in benzylic position; z = no. of bpy arms deuterated in aromatic position. [f]Sample standard deviation (using Bessel's correction) in parentheses. [g]Calculated using the parameters obtained from the global fitting procedure (see Table 3). [h]Ref 11b.

Table 3. Quenching Rate Differences Δk for Benzylic and Aromatic C−(H/D) Oscillator Groups in $[D_x]$-Ln[a]

Ln	k_0 [ms^{-1}][b]	$\Delta k_{Bn\text{-}NO}$ [ms^{-1}][b]	$\Delta k_{Ar\text{-}NO}$ [ms^{-1}][b]	Δk_{Bn} [ms^{-1}][b]	Δk_{Ar} [ms^{-1}][b]	$\Delta k_{Ar}/g$ [ms^{-1}][c]
Nd	1343(6)	253(8)	14(8)	309(4)	55(2)	38
Er	567(7)	59(12)	25(12)	89(4)	29(3)	19
Yb	87.58(2)	20.49(6)	3.14(7)	23.64(1)	2.83(2)	1.85

[a]Standard error in parentheses. [b]Global fitting of the lifetime data to: $k_{obs} = k_0 - w\,\Delta k_{Bn\text{-}NO} - x\,\Delta k_{Ar\text{-}NO} - y\,\Delta k_{Bn} - w\,\Delta k_{Ar}$; with w, x, y, z as defined in Table 2; $k_0 = k_{obs}$ ($[\mathbf{D_0}]$-**Ln**) as an optimized parameter; $\Delta k_{Bn\text{-}NO}$ and Δk_{Bn} = quenching rate difference (C−H minus C−D) for the two benzylic methylene groups of one cryptand arm (with index "NO": bpy-*N*,*N*′-dioxide); $\Delta k_{Ar\text{-}NO}$ and Δk_{Ar} = quenching rate difference (C−H minus C−D) for the six aromatic C−(H/D) oscillators of one cryptand arm (with index "NO": bpy-*N*,*N*′-dioxide). Fitting on χ^2 using weighting factors $w_i = 1/s_i^2$ with s_i = sample standard deviation (see Table 2). [c]For values of g, see Table 1.

lanthanoids, is a further indication that the chloride is retained in the first coordination sphere of the lanthanoid in methanolic solution.

2.4. Near-IR Vibrational Spectroscopy. The measurement of overtones of C−H(D) oscillators is challenging due to a number of intrinsic problems. Since the molar extinction coefficients quickly become very small with increasing vibrational quantum number n, high concentrations of the analytes are required for accurate quantitative data. This is particularly the case for C−D oscillators because they generally exhibit even lower absorptivities than analogous protiated moieties. In addition to this fundamental difficulty of weak absorptivities, the list of possible solvents is also rather limited because most media themselves exhibit strong absorption in certain parts of the near-IR region. Especially problematic in this respect are solvents with X−H moieties (X = C, O) which makes their use all but impossible. Since the cryptates are only soluble enough in polar media like water or alcohols, the most practical solvent for the lanthanoid cryptates proved to be CD_3OD. In the course of our initial near-IR measurements, two things became obvious. First, the lanthanoid cryptates as synthesized were not suitable because of the presence of protiated species like MeOH and H_2O in the bulk material, which affected the spectra very negatively. Second, although it was possible to measure C−H overtone bands, we were not able to reproducibly measure higher C−D overtones because of the weak absorptions even at concentrations near the solubility limit in CD_3OD. As a consequence of these orienting trials, we resynthesized the nondeuterated cryptate $[\mathbf{D_{solvent}}]$-**Lu** (see the Supporting Information) on a relatively large scale using CD_3OD (instead of CH_3OH) during the final precipitation step. Near-IR absorption measurements with $[\mathbf{D_{solvent}}]$-**Lu** were successful for the second (n = 3) and third (n = 4) overtones (Figure 5). Both regions show a pronounced and rather sharp maximum at higher wavenumbers which was assigned as the

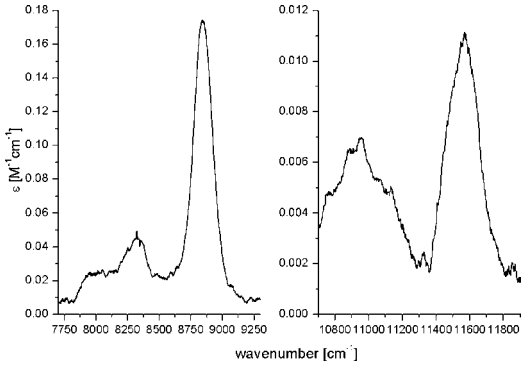

Figure 5. Near-IR absorption spectrum of $[\mathbf{D_{solvent}}]$-**Lu** (CD_3OD, c = 11.2 mM, d = 5 cm) in the overtone region of n = 3 (left) and n = 4 (right).

aromatic C−H absorptions (Figure 5). In order to extract the absorption bands originating from the aromatic oscillators, the spectra were deconvoluted with a series of Lorentzian functions (see Supporting Information). The reconstructed aromatic bands showed peak maxima and integrated molar absorptivities given in Table 4.

Since we could only acquire this very limited amount of data on the vibrational overtones in the cryptates, we decided to

Table 4. Maxima and Molar Absorptivities of Aromatic C−H Overtones in $[\mathbf{D_{solvent}}]$-Lu (CD_3OD, c = 11.2 mM)

n	$\tilde{\nu}_n^{max}$ [cm^{-1}]	$\int \varepsilon_n(\tilde{\nu})\,d\tilde{\nu}$ [M^{-1} cm^{-2}]
3	8843	43.7[a]
4	11569	3.59[a]

[a]After reconstruction of the peaks by fitting procedures (see the Supporting Information).

dx.doi.org/10.1021/ja307339f | J. Am. Chem. Soc. 2012, 134, 16413−16423

perform additional and extended measurements on simpler model systems. For this, we chose the purely organic isotopologues of 6,6′-dimethyl-2,2′-bipyridine **bpy** and [$\mathbf{D_{12}}$]-**bpy** and of the corresponding *N*,*N*′-dioxide **bpyO$_2$** and [$\mathbf{D_{12}}$]-**bpyO$_2$** (Chart1). Three of the four compounds (**bpy**, **bpyO$_2$**, [$\mathbf{D_{12}}$]-**bpyO$_2$**) are intermediates of the cryptate synthesis and were therefore available in the necessary amounts and purity. [$\mathbf{D_{12}}$]-**bpy** was prepared by reduction of [$\mathbf{D_{12}}$]-**bpyO$_2$** (see Supporting Information). All four species are highly soluble in CD_3OD and also in $CDCl_3$ which is a more suitable solvent than CD_3OD for near-IR absorption measurements due to its reduced absorption, especially in the region of the first C−H overtones (ca. 5500−6500 cm^{-1}). In order to see whether the use of $CDCl_3$ would change the absorption behavior compared to CD_3OD, we performed initial measurements with **bpy** and **bpyO$_2$** in both solvents in the overtone regions n = 2−4 (Figures 6 and 7). The obtained spectra in CD_3OD and $CDCl_3$ were almost identical in terms of band position and shape as well as intensity. In addition, the spectra for **bpy** and **bpyO$_2$** show subtle differences but are very similar overall.

Chart 1. Model Compounds for the Near-IR Vibrational Absorption Measurements

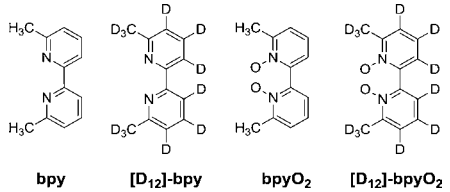

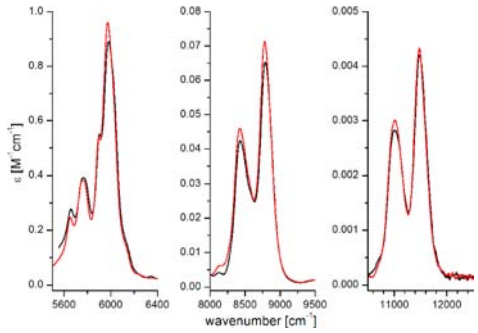

Figure 6. Near-IR absorption spectra of **bpy** in CD_3OD (black, c = 320 mM, d = 5 cm) and $CDCl_3$ (red, c = 338 mM, d = 5 cm) in the regions n = 2−4.

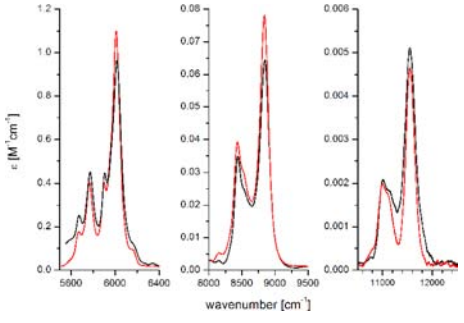

Figure 7. Near-IR absorption spectra of **bpyO$_2$** in CD_3OD (black, c = 286 mM, d = 5 cm) and $CDCl_3$ (red, c = 285 mM, d = 5 cm) in the regions n = 2−4.

Since the situation in $CDCl_3$ seemed to reflect the one in CD_3OD very well, we carried out further near-IR measurements in $CDCl_3$. With the use of $CDCl_3$, the measurement of the deuterated analogues [$\mathbf{D_{12}}$]-**bpy** and [$\mathbf{D_{12}}$]-**bpyO$_2$** were possible for the second and third overtones (n = 3−4). All spectra were deconvoluted with a series of Lorentzian functions in order to extract the aromatic oscillators. For the regions of the deuterated species, where $CDCl_3$ itself shows weak absorption, the solvent peaks had to be explicitely modeled by the addition of Lorentzian functions with negative amplitudes (see Supporting Information). The results of these reconstructive peak extraction procedures for the aromatic C−(H/D) oscillators are shown in Figures 8 and 9 and the data are summarized in Table 5.

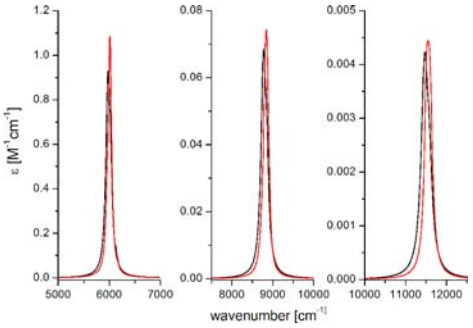

Figure 8. Reconstructed near-IR absorption spectra for the aromatic C−H oscillators of **bpy** (black) and **bpyO$_2$** (red) in $CDCl_3$ in the regions n = 2−4.

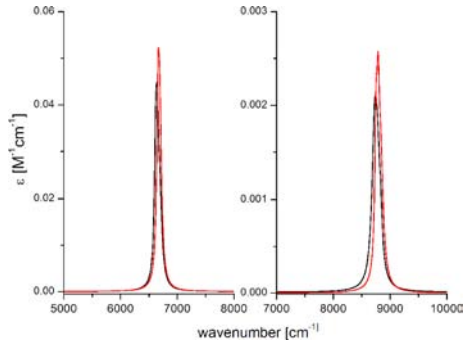

Figure 9. Reconstructed near-IR absorption spectra for the aromatic C−D oscillators of [$\mathbf{D_{12}}$]-**bpy** (black) and [$\mathbf{D_{12}}$]-**bpyO$_2$** (red) in $CDCl_3$ in the regions n = 3−4.

Table 5. Peak Maxima Positions and Integrated Molar Absorptivities of Aromatic C−H and C−D Overtones of the Model Compounds bpy, [$\mathbf{D_{12}}$]-bpy, bpyO$_2$, and [$\mathbf{D_{12}}$]-bpyO$_2$[a]

		[D_x]-bpy		[D_x]-bpyO$_2$	
	n	$\tilde{\nu}_n$ [cm^{-1}]	$\int \varepsilon_n(\tilde{\nu})\, d\tilde{\nu}$ [M^{-1} cm^{-2}]	$\tilde{\nu}_n$ [cm^{-1}]	$\int \varepsilon_n(\tilde{\nu})\, d\tilde{\nu}$ [M^{-1} cm^{-2}]
C−H	2	5973	163	6009	142
([D_0])	3	8778	17.8	8840	15.3
	4	11480	1.56	11555	1.32
C−D	3	6638	6.66	6667	6.67
([D_{12}])	4	8738	0.47	8781	0.46

[a]After deconvolution of the peaks by fitting procedures (see the Supporting Information).

dx.doi.org/10.1021/ja307339f | J. Am. Chem. Soc. 2012, 134, 16413−16423

As can be seen in Table 5, the integrated intensities of the corresponding vibrational bands in $[D_x]$-**bpy** and $[D_x]$-**bpyO$_2$** are the same within the experimental uncertainties. In contrast, the energies of the oscillators situated on the bpy moieties are slightly lower compared to the analogous ones residing on the corresponding *N*,*N*′-dioxide units. As a check on the validity of using the model compounds in $CDCl_3$ (see Chart 1) instead of the lanthanoid cryptates in CD_3OD, we simulated the aromatic C−H absorption of a nondeuterated tris(bipyridine) cryptate with the reconstructed aromatic absorption bands of **bpy** and **bpyO$_2$**. For this purpose, we added the corresponding bands of this hypothetical three component cryptate (i.e., 2 × **bpy** + 1 × **bpyO$_2$**) and compared it to the reconstructed aromatic C−H absorptions of the actually measured cryptate $[D_{solvent}]$-**Lu**. The spectra for the second and third overtones are in good agreement within the experimental uncertainties, both in terms of peak position and intensity, proving the validity of our approach (Figure 10).

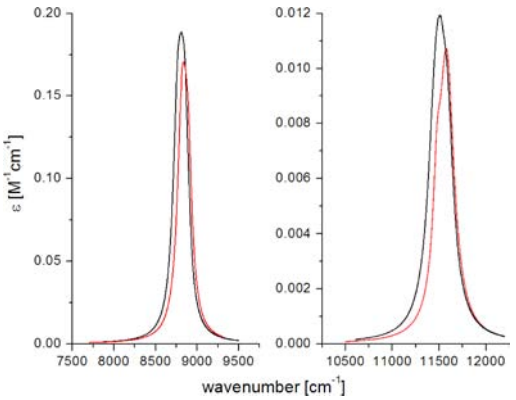

Figure 10. Reconstructed near-IR absorption spectra for the aromatic C−H oscillators of $[D_{solvent}]$-**Lu** in CD_3OD (red) and a hypothetical cryptate composed of 2 × **bpy** and 1 × **bpyO$_2$** in CD_3OD (black) in the regions n = 3−4.

3. DISCUSSION

3.1. Overtone Energies. Aromatic C−H oscillators have been investigated in the past for a number of pyridine-containing species. The vibrational overtone structure can be well described with a local-mode, anharmonic Morse oscillator model.[21] In particular, it has been observed in a number of instances (e.g., pyridine and 2,6-lutidine) that the three C−H oscillators in 3-, 4-, and 5-position are very similar and their vibrational signatures can usually not be resolved.[22] In the Morse model, the energy $\tilde{\nu}_n$ (in the wavenumber scale) of the overtone with quantum number n depends on the frequency $\tilde{\nu}_0$ of the local-mode fundamental vibration and the anharmonicity parameter x according to the following expression:

$$\frac{\tilde{\nu}_n}{n} = \tilde{\nu}_0 - (n+1)x \tag{7}$$

The Morse parameters can be determined experimentally by a Birge−Sponer plot. A linear fit of a plot $(\tilde{\nu}_n/n)$ versus $(n+1)$ gives $\tilde{\nu}_0$ as the y-axis intercept and the slope $-x$. The overtone positions for all model compounds can be found in Tables 4 and 5. Table 6 contains a summary of the results of the determinations for different oscillators (see Supporting Information for Birge−Sponer plots).

Table 6. Local-Mode, Morse Parameters for Aromatic C−(H/D) Oscillators: Local Model Fundamental Frequency $\tilde{\nu}_0$, Anharmonicity x, and the Calculated Anharmonicity Ratio k

	$\tilde{\nu}_0$ [cm^{-1}]	x [cm^{-1}]	$k = \tilde{\nu}_0/x$
$[D_{solvent}]$-**Lu** (C−H)	3169	55	58
bpy (C−H)	3161	58	55
bpyO$_2$(C−H)	3178	58	55
$[D_{12}]$-**bpy** (C−D)	2325	28	83
$[D_{12}]$-**bpyO$_2$** (C−D)	2331	27	86

The obtained Morse parameters for the aromatic C−H oscillators (Table 6, rows 1−3) are very similar to previously reported values for the three oscillators in 3-, 4-, and 5-positions of pyridine and 2,6-lutidine ($\tilde{\nu}_0 \approx 3140-3160$ cm^{-1} and x ≈ 56−60 cm^{-1})[22a,b] or even the local mode oscillators in benzene ($\tilde{\nu}_0$ = 3150 cm^{-1} and x = 60 cm^{-1}).[23] The corresponding C−D local modes also show good agreement with other aromatic species, like the aromatic overtones of $[D_8]$-toluene ($\tilde{\nu}_0$= 2334 cm^{-1} and x = 30 cm^{-1}).[24] This remarkable insensitivity of these local mode oscillators to the nature of the specific aromatic system implies that our analysis in terms of C−(H/D) overtone positions should have some general applicability with respect to all kinds of aromatic ligand systems for the complexation of lanthanoids. Especially the size of the anharmonicity parameter $x \approx 58$ cm^{-1} should be of very general validity, while the fundamental frequencies can vary slightly with the specific molecular structure. It also implies that it is a valid assumption that overtone positions should not vary with the nature of the lanthanoid in the different cryptates.

3.2. Overtone Intensities. The intensities of the different overtones in **bpy**, $[D_{12}]$-**bpy**, **bpyO$_2$**, and $[D_{12}]$-**bpyO$_2$** were determined by integration over the reconstructed, aromatic C−(H/D) bands (Table 5). Under certain assumptions (only mechanical anharmonicity, large values for k, transition dipole moment proportional to nuclear displacement), the following relationship holds for the overtone intensity I_n of a Morse oscillator.[21a]

$$I_n \propto \frac{n!}{n^2} k^{1-n} \tag{8}$$

with the anharmonicity ratio $k = \tilde{\nu}_0/x$. The intensity ratio between corresponding C−H and C−D overtones is

$$\frac{I_n^{H}}{I_n^{D}} \propto \left(\frac{k^{D}}{k^{H}}\right)^{n-1} \tag{9}$$

with k^D/k^H (see Table 5) and $(n-1)$ both >1. Therefore, the intensity ratio in eq 9 becomes successively larger with increasing vibrational quantum number n. In other words, because of its lower anharmonicity, the intensities of the C−D oscillators should go down more quickly than the ones for the analogous C−H modes. Semilogarithmic plots of the integrated absorptivities of our model compounds against the vibrational quantum number n indeed show this trend (Figure 11). The intensity data for the C−H oscillators in these plots can be fitted well with a linear function. The lines through the two data points for each C−D mode shows a steeper negative slope, a clear manifestation of this effect (Table 7). Equation 8, however, implies a certain curvature of the exponential decrease of the overtone intensities for a particular oscillator. For example, the predicted drop in intensity going from the first (n

dx.doi.org/10.1021/ja307339f | J. Am. Chem. Soc. 2012, 134, 16413−16423

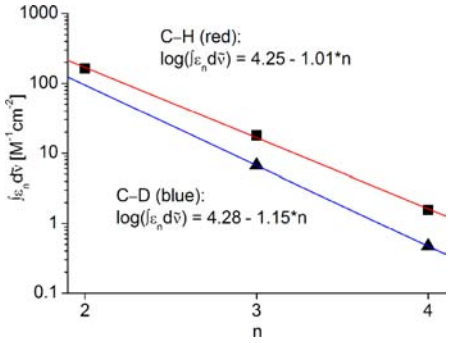

Figure 11. Semilogarithmic plot of the integrated absorbances for aromatic C−H (squares) and C-D (triangles) oscillators in **bpy** and $[\mathbf{D_{12}}]$**-bpy** against the quantum number n.

Table 7. Parameters for the Linear Functions of the Integrated Absorptivities ($\log(\int \varepsilon_n(\tilde{\nu})\, d\tilde{\nu}) = a_1 - a_2 \cdot n$)

	a_1 [M^{-1} cm^{-2}]	a_2 [M^{-1} cm^{-2}]
bpy (C−H)	4.25	1.01
bpyO$_2$ (C−H)	4.20	1.02
$[\mathbf{D_{12}}]$**-bpy** (C−D)	4.28	1.15
$[\mathbf{D_{12}}]$**-bpyO$_2$** (C−D)	4.30	1.16

= 2) to the second (n = 3) C−H overtone in **bpy** should be approximately 40-fold (Table 8: 100% → 2.4%). In reality, the

Table 8. Experimental Overtone Intensities of bpy and $[\mathbf{D_{12}}]$-bpy and Calculated, Relative Intensity Ratios

	n	$\int \varepsilon_n(\tilde{\nu})\, d\tilde{\nu}$ [M^{-1} cm^{-2}]	experimental relative intensity ratio	calculated relative intensity ratio[a]
C−H[b]	2	163	100%	100%
($[D_0]$)	3	17.8	11%	2.4%
	4	1.56	0.96%	0.099%
C−D[c]	3	6.66	100%	100%
($[D_{12}]$)	4	0.47	7.1%	2.7%

[a]Calculated using eq 8. [b]k = 55 (Table 6). [c]k = 83 (Table 6).

measured decrease is much less pronounced (Table 8: 100% → 11%). This phenomenon is valid for all oscillators investigated and could have its origin in a strong anharmonic electronic component or considerable nonlinearities between transition dipole moments and nuclear displacement.

3.3. Spectral Overlap Factors. Having established the vibrational overtone bands for the aromatic C−(H/D) oscillators (see Section 2.4), we calculated the SOIs for the different lanthanoids as defined in eq 3. This was not possible for neodymium with the relevant energy gap being $^4F_{3/2}$−$^4I_{15/2}$ (ca. 5400 cm^{-1}, ca. 1850 nm) because we could not directly measure the corresponding emission band due to instrument limitations. For Pr, Er, and Yb, on the other hand, we determined the SOIs of the suitable overtones with the lanthanoid transition corresponding to the relevant energy gap (Pr, $^1D_2$ → $^1G_4$; Er, $^4I_{13/2}$ → $^4I_{15/2}$; Yb, $^2F_{5/2}$ → $^2F_{7/2}$) by constructing the integrand function of the overlap integral and subsequent numerical integration (see the Supporting Information).

Under the assumption that k_r, κ, r in eq 2 are approximately the same for corresponding C−H and C−D, the ratio ζ of the SOIs for these isotopologic oscillator moieties directly reflects the ratio of the corresponding nonradiative deactivation rates. With this definition, ζ could be called "quenching attenuation factor".

$$\zeta = \frac{k_{nr}^{H}}{k_{nr}^{D}} = \frac{\int I_{norm}(\tilde{\nu}) \cdot \varepsilon_{vib}^{H}(\tilde{\nu}) \cdot \tilde{\nu}^{-4}\, d\tilde{\nu}}{\int I_{norm}(\tilde{\nu}) \cdot \varepsilon_{vib}^{D}(\tilde{\nu}) \cdot \tilde{\nu}^{-4}\, d\tilde{\nu}} \quad (10)$$

The numerical value of ζ determines the achievable luminescence enhancement by deuteration. Interestingly, the situation with respect to ζ is very different for the three lanthanoids Pr, Er, and Yb (Table 9). Yb shows large ζ values

Table 9. Spectral Overlap Integrals (SOI) and Quenching Attenuation Factor ζ for the Lanthanoids Pr, Er, and Yb with the Aromatic C−(H/D) Oscillators in bpy, $[\mathbf{D_{12}}]$-bpy, bpyO$_2$, and $[\mathbf{D_{12}}]$-bpyO$_2$

	SOI $[\mathbf{D_x}]$**-bpy** [M^{-1} cm^3]	SOI $[\mathbf{D_x}]$**-bpyO$_2$** [M^{-1} cm^3]
Pr/C−H (n = 2)[a]	1.41×10^{-18}	1.07×10^{-18}
Pr/C−D (n = 3)[a]	2.78×10^{-18}	3.12×10^{-18}
$\zeta = \frac{SOI^{C-H}}{SOI^{C-D}}$	0.507	0.343
Er/C−H (n = 2)[b]	6.04×10^{-18}	5.03×10^{-18}
Er/C−D (n = 3)[b]	5.92×10^{-18}	5.52×10^{-18}
$\zeta = \frac{SOI^{C-H}}{SOI^{C-D}}$	1.02	0.911
Yb/C−H (n = 3)[c]	3.66×10^{-20}	2.52×10^{-20}
Yb/C−D (n = 4)[c]	6.89×10^{-22}	6.73×10^{-22}
$\zeta = \frac{SOI^{C-H}}{SOI^{C-D}}$	53.1	37.4

[a]Pr: $^1D_2$ → $^1G_4$. [b]Er: $^4I_{13/2}$ → $^4I_{15/2}$. [c]Yb: $^2F_{5/2}$ → $^2F_{7/2}$.

for the aromatic oscillators (ζ = 53.1 for $[\mathbf{D_x}]$**-bpy** and ζ = 37.4 for $[\mathbf{D_x}]$**-bpyO$_2$**). In contrast to this, the values for Er are around $\zeta \approx 1$, while for Pr, ζ is even below 1. In other words, deuteration decreases nonradiative deactivation considerably for Yb, while it does not make much of a difference for Er, and is even detrimental for Pr ($k_{nr}^{D} > k_{nr}^{H}$). The rather surprising result for Pr has been observed experimentally by us recently in a very similar tris(bipyridine) ligand system.[11c] The fact that we can explain this behavior with the determined ζ values provides strong evidence for the validity and predictional power of the present study.

3.4. Absolute Quenching Rates. In Section 2.3, we have determined the nonradiative deactivation rate differences Δk_{nr}^{H-D} for the various oscillator groups in the cryptates $[\mathbf{D_x}]$-**Ln** (Table 3). With the quenching attenuation factors ζ for Er and Yb from the previous section (Table 9), it is possible to calculate absolute quenching rates for both isotopologic, aromatic oscillator types.

$$\Delta k_{nr}^{H-D} = k_{nr}^{H} - k_{nr}^{D} \quad (11)$$

From eq 10 and 11, we obtain the absolute quenching rates for the isotopologic oscillators:

$$k_{nr}^{H} = \Delta k_{nr}^{H-D}\left(\frac{\zeta}{\zeta - 1}\right) \quad \text{and} \quad k_{nr}^{D} = \Delta k_{nr}^{H-D}\left(\frac{1}{\zeta - 1}\right) \quad (12)$$

Table 10 shows as an example the absolute nonradiative deactivation rates for the C−(H/D) oscillators groups in **bpy**. For Yb, the differences are expectedly large (2.88 ms^{-1} vs 0.05 ms^{-1}). The absolute values k_{nr} are specific for a set of oscillators at certain distances (here in the bpy parts of $[\mathbf{D_x}]$**-Yb** with

dx.doi.org/10.1021/ja307339f | J. Am. Chem. Soc. 2012, 134, 16413−16423

Table 10. Absolute quenching rates k for aromatic C−(H/D) oscillator groups in $[D_x]$-bpy

	$[D_x]$-bpy		
Ln	Δk^{bpy} $[ms^{-1}]^a$	k_{nr}^{H} $[ms^{-1}]$	k_{nr}^{D} $[ms^{-1}]$
Er	29	$(1479)^b$	$(1450)^b$
Yb	2.83	2.88	0.05

[a]See Table 3. [b]Values afflicted with large uncertainties (see text).

distances r as listed in Table 1) but can easily be converted to other distances by the relationship $k_{nr} \propto r^{-6}$.

For Er, the calculation can also be performed and yields high values around 1450−1479 ms^{-1} for both isotopologic oscillators. These values, however, are not very reliable since small errors in the associated ζ values lead to huge potential errors in the absolute quenching rates. Consequently, it appears more reasonable to only qualitatively conclude on the basis of the quenching attenuation factors ($\zeta \approx 1$) that aromatic deuteration does not affect nonradiative deactivation in a significant, positive way.

3.5. Empirical SOI Approximation. As mentioned in the introduction, the Förster-type spectral overlap integral SOI as defined in eq 3 requires a detailed knowledge of the bandshapes of the lanthanoid emission and the vibrational overtones of the oscillators X−H. The emission is usually not problematic because it is easily obtained for most lanthanoids and does not change much with the chemical surrounding. The energy and intensity of the vibrational overtones, in general, can change dramatically depending on the exact nature of the oscillator. The situation for the aromatic C−(H/D) modes in $[D_x]$-**Ln**, however, is different. We have shown that these oscillators can be well described by a local-mode Morse model and that the position and intensity does not change substantially with the chemical environment, which permitted us the use of simple bipyridine model compounds for our investigation instead of the actual cryptates (see the discussion in Section 2.4). Under these circumstances (fixed lanthanoid emission bands and fixed overtone positions governed by the Morse relation in eq 7), it is possible to determine the energetic difference Δ between the lanthanoid emission and the relevant overtone without the exact knowledge of the near-IR absorption spectrum of the oscillators. Δ, together with the widths of the bands involved, should in large part be responsible for the extent of spectral overlap. Malta et al. have used this parameter in the past to theoretically derive an expression for a similar overlap integral F between two idealized Gaussian bands g_D and g_A:[25]

$$F = \int g_D(E)\cdot g_A(E)\,dE \approx \frac{\sqrt{\ln 2}}{\pi\cdot\hbar\cdot\gamma_D}\, e^{-\ln 2(\Delta/\hbar\cdot\gamma_D)^2} \qquad (13)$$

where Δ is the spectral separation introduced above and γ_D is the full width at half-maximum (fwhm) of the Gaussian g_D. Equation 13 holds if the fwhm of Gaussian g_A is much smaller than γ_D. This seems to be a good approximation for energy transfer processes from a ligand-centered charge transfer state (with a large fwhm) to a lanthanoid-centered state (which has a very small fwhm).[25] In the case of multiphonon relaxation discussed here, this model is problematic. For one, the mathematical treatment of the Förster-type integral SOI in eq 3 is greatly complicated by the presence of the factor $\tilde{\nu}^{-4}$ in the integrand compared to the overlap integral F in eq 13. In addition, the band widths of the lanthanoid emission and the different vibrational overtones are of similar magnitude and neither can be neglected for any mathematical approximation procedure. The knowledge of the exact aromatic C−(H/D) overtone band shapes and intensities for the bipyridine building blocks **bpy**, $[D_{12}]$-**bpy**, **bpyO$_2$**, and $[D_{12}]$-**bpyO$_2$**, however, makes it possible to quantitatively investigate the impact that a spectral offset Δ has on the magnitude of SOI. For this purpose, we artificially shifted the relevant overtones (with constant shape and intensity) relative to a fixed, specific lanthanoid emission band from $\Delta = 0$ cm^{-1} (i.e., emission and overtone maximum at the same energy → maximum spectral overlap) systematically to higher Δ. For each value of Δ, we calculated the corresponding SOI. In the case of Yb, where two maxima are present in the same band (see Figure 4), we chose the local maximum with the lowest energy (at ca. 9770 cm^{-1}) as reference energy for the calculation of Δ because this is the most consequential for overlap with an overtone (which usually is energetically below the emission energy). As an example, Figure 12 shows the corresponding data for the variation between the SOIs of aromatic C−H oscillators and the Pr band $^1D_2 \rightarrow {}^1G_4$ (for all other graphs see the Supporting Information).

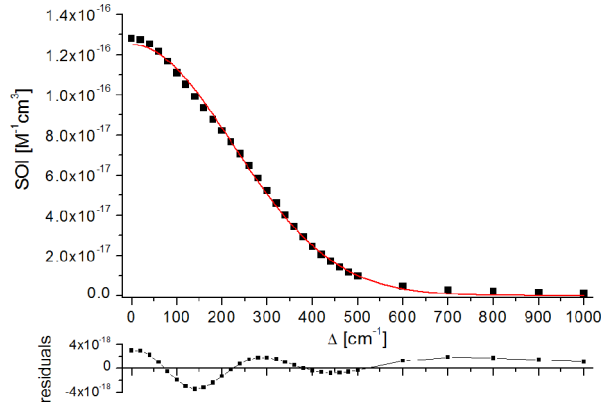

Figure 12. Spectral overlap integral (SOI) between the $^1D_2 \rightarrow {}^1G_4$ emission band in $[D_{30}]$-**Pr** and the first overtone ($n = 2$) of aromatic C−H oscillators in **bpy** versus the peak separations Δ of these two bands, Gaussian fit in red.

All plots SOI versus Δ show a strong resemblance to simple Gaussian distribution profiles. This is striking, because our approach does not require any assumption on the band shapes involved (see the approximations for the derivation of F in eq 13) and seems to work even for lanthanoid emission bands that are far from being Gaussian themselves (cf. Yb or Er in Figure 4). This allows a very convenient empirical approximation of the complicated functional definition of the spectral overlap integral in eq 3. We chose the following Gaussian with the variable Δ:

$$SOI = \int I_{norm}(\tilde{\nu})\cdot\varepsilon_{vib}(\tilde{\nu})\cdot\tilde{\nu}^{-4}\,d\tilde{\nu} \approx a\, e^{(-1/2)(\Delta/b)^2} \qquad (14)$$

This purely empirical model has only two fit-parameters, the amplitude parameter a and the width parameter b. Tables 11 and 12 show the results of the Gaussian fitting procedures for different lanthanoids and overtones. The parameters a and b obtained by fitting of the data for different lanthanoids and overtones show some interesting trends. The value a seems to be of comparable magnitude for the overlap of a specific overtone with any lanthanoid. For example, the values of a for

dx.doi.org/10.1021/ja307339f | J. Am. Chem. Soc. 2012, 134, 16413−16423

Table 11. Parameters for the Gaussian Fits of the Spectral Overlap Integral SOI Variation with the Spectral Separation Δ for the C−(H/D) Oscillators in $[D_x]$-bpy

	a [M^{-1} cm^3][a]	b [cm^{-1}][a]
Pr/C−H (n = 2)[b]	1.2×10^{-16}	223
Pr/C−D (n = 3)[b]	5.3×10^{-18}	219
Er/C−H (n = 2)[c]	1.6×10^{-16}	264
Er/C−D (n = 3)[c]	6.7×10^{-18}	261
Yb/C−H (n = 3)[d]	1.6×10^{-18}	272
Yb/C−D (n = 4)[d]	4.2×10^{-20}	262

[a]SOI ≈ $a \exp\{-0.5(\Delta/b^2)\}$. [b]Pr: $^1D_2 \rightarrow {}^1G_4$. [c]Er: $^4I_{13/2} \rightarrow {}^4I_{15/2}$. [d]Yb: $^2F_{5/2} \rightarrow {}^2F_{7/2}$.

Table 12. Parameters for the Gaussian Fits of the Spectral Overlap Integral SOI Variation with the Spectral Separation Δ for the C−(H/D) Oscillators in $[D_x]$-bpyO$_2$

	a [M^{-1} cm^3][a]	b [cm^{-1}][a]
Pr/C−H (n = 2)[b]	1.1×10^{-16}	208
Pr/C−D (n = 3)[b]	5.3×10^{-18}	216
Er/C−H (n = 2)[c]	1.4×10^{-16}	246
Er/C−D (n = 3)[c]	6.7×10^{-18}	257
Yb/C−H (n = 3)[d]	1.4×10^{-18}	247
Yb/C−D (n = 4)[d]	4.3×10^{-20}	260

[a]SOI ≈ $a \exp\{-0.5(\Delta/b^2)\}$. [b]Pr: $^1D_2 \rightarrow {}^1G_4$. [c]Er: $^4I_{13/2} \rightarrow {}^4I_{15/2}$. [d]Yb: $^2F_{5/2} \rightarrow {}^2F_{7/2}$.

the combinations Pr/C−H (n = 2) and Er/C−H (n = 2) in Table 11 are very similar (Pr, 1.2×10^{-16} M^{-1} cm^3 vs Er, 1.6×10^{-16} M^{-1} cm^3). This is not surprising since it reflects for the most part the intensity of the specific overtone involved (here n = 2 in both cases). The variation in b for the same combination (Pr, b = 223 cm^{-1} vs Er, b = 264 cm^{-1}) seems to be mainly connected to the bandwidth of the characteristic lanthanoid emission band. The fact that b has an almost identical magnitude for corresponding isotopologic oscillators with the same lanthanoid (e.g., for Pr in Table 11, b_{C-H} = 223 cm^{-1} vs b_{C-D} = 219 cm^{-1}) points in the same direction.

While the values for a and b, in general, will vary for different lanthanoid complexes, it is highly likely that the SOIs associated with a specific structural element can equally be described by this simple, empirical Gaussian model. With a more comprehensive collection of empirical data for different oscillators in the future, this promises a very simple predictive model for the estimation of C−(H/D) nonradiative deactivation rates in molecular lanthanoid complexes, similar in practical appeal to the EGL.

4. CONCLUSION

In summary, we have applied a combination of experimental and theoretical methods to comprehensively study the structural and photophysical properties of the near-IR luminescent lanthanoid cryptates $[D_x]$-**Ln** and the impact that aromatic C−(H/D) oscillators have on multiphonon relaxation. In particular, we could:

(i) accurately establish the distances Ln−(H/D) in $[D_x]$-**Ln** in methanolic solution.
(ii) measure the nonradiative deactivation rate differences Δk_{nr} for four different oscillator groups upon deuteration.
(iii) quantify the energy and the intensity of the relevant vibrational overtones of aromatic C−(H/D) oscillators.
(iv) confirm that the energetic positions of the overtones deviate considerably from the ones that are predicted by a harmonic oscillator model, which is still the overwhelmingly prevalent theoretical framework for the discussion of multiphonon relaxation. The aromatic overtones can successfully be modeled as local-mode, anharmonic Morse oscillators and the anharmonicity parameters for the isotopologic C−(H/D) modes were determined. The anharmonicities agree well with previously obtained data on simple aromatic compounds which suggests that these parameters will be generally applicable for a wide variety of ligands with aromatic units.
(v) quantify the spectral overlap integrals (SOIs) of the aromatic C−(H/D) overtones with the relevant emission bands of Pr, Er, and Yb and consequently calculate some absolute rates for nonradiative deactivation.
(vi) propose that appropriate Gaussian relationships (as a function of the spectral separation Δ between vibrational overtones and lanthanoid electronic levels) are good empirical approximations for the calculation of spectral overlap integrals (SOIs).

The present results for the first time provide a realistic and generally applicable framework for nonradiative deactivation of lanthanoid electronic states by highly anharmonic, aromatic C−(H/D) oscillators. The obtained insights will considerably enhance the conceptual understanding of multiphonon relaxation and be of great value for the design and optimization of new and improved molecular near-IR lanthanoid luminophores.

■ ASSOCIATED CONTENT

Supporting Information

Full experimental details for synthetic procedures and analytical characterization for all new compounds, details for the spectroscopic measurements (NMR, near-IR absorption, luminescence), extended tables for data analysis. This material is available free of charge via the Internet at http://pubs.acs.org.

■ AUTHOR INFORMATION

Corresponding Author

carlos.platas.iglesias@udc.es; michael.seitz@rub.de

Notes

The authors declare no competing financial interest.

■ ACKNOWLEDGMENTS

This article is dedicated to Professor Kenneth N. Raymond (UC Berkeley). C.P.-I. thanks Centro de Supercomputación de Galicia (CESGA) for providing the computer facilities. M.S. thanks Prof. Dr. Nils Metzler-Nolte (Ruhr-University Bochum) for his continued support. Financial support is gratefully acknowledged from: DFG (Emmy Noether Fellowship M.S.), Fonds der Chemischen Industrie (Liebig Fellowship for M.S. and predoctoral fellowships for C.D. and N.A.), Int. Max Planck Research School in Chemical Biology (predoctoral fellowship for C.B.), Research Department Interfacial Systems Chemistry (Ruhr-University Bochum).

■ REFERENCES

(1) (a) Englman, R.; Jortner, J. *Mol. Phys.* **1970**, *18*, 145. (b) Robinson, G. W.; Frosch, R. P. *J. Chem. Phys.* **1963**, *38*, 1187.

(c) Henry, B. R.; Siebrand, W. In *Organic Molecular Photophysics (Vol. I)*; Birks, J. B., Ed.; Wiley: London, 1973; p 153.
(2) (a) Basiev, T. T.; Orlovskii, Yu. V.; Pukhov, K. K.; Auzel, F. *Laser Phys.* **1997**, *7*, 1139. (b) Malkin, B. Z. In *Spectroscopic Properties of Rare Earths in Optical Materials (Springer Series in Material Science Vol. 83)*; Liu, G., Jacquier, B., Eds.; Springer: Hamburg, 2005; p 131.
(3) (a) Caspar, J. V.; Kober, E. M.; Sullivan, B. P.; Meyer, T. J. *J. Am. Chem. Soc.* **1982**, *104*, 630. (b) Kober, E. M.; Caspar, J. V.; Lumpkin, R. S.; Meyer, T. J. *J. Phys. Chem.* **1986**, *90*, 3722. (c) Casper, J. V.; Meyer, T. J. *Inorg. Chem.* **1983**, *105*, 2444.
(4) (a) Bünzli, J.-C. G.; Eliseeva, S. V. *J. Rare Earths* **2010**, *28*, 824. (b) Comby, S.; Bünzli, J.-C. G. In *Handbook on the Physics and Chemistry of Rare Earths*; Gschneidner, K. A., Jr., Bünzli, J.-C. G., Pecharsky, V. K., Eds.; Elsevier: Amsterdam, 2007; Vol. *37*, p 217; (c) Werts, M. H. V. In *Lanthanide Luminescence* (Springer Series on Fluorescence 7); Hänninen, P.; Härma, H., Eds.; Springer: Berlin, 2011; p 133.
(5) (a) Sveshnikova, E. B.; Ermolaev, V. L. *Opt. Spectrosc.* **2011**, *111*, 34. (b) Ermolaev, V. L.; Sveshnikova, E. B. *Russ. Chem. Rev.* **1994**, *63*, 905.
(6) Förster, T. *Ann. Phys.* **1948**, *437*, 55.
(7) Supkowski, R. M.; Horrocks, W. D., Jr. *Inorg. Chim. Acta* **2002**, *340*, 44.
(8) Beeby, A.; Clarkson, I. M.; Dickins, R. S.; Faulkner, S.; Parker, D.; Royle, L.; de Sousa, A. S.; Williams, J. A. G.; Woods, M. *J. Chem. Soc., Perkin Trans. 2* **1999**, 493.
(9) (a) Quochi, F.; Orru, R.; Cordella, F.; Mura, A.; Bongiovanni, G.; Artizzu, F.; Deplano, P.; Mercuri, M. L.; Pilia, L.; Serpe, A. *J. Appl. Phys.* **2006**, *99*, 053520.
(10) (a) Monguzzi, A.; Milani, A.; Lodi, L.; Trioni, M. I.; Tubino, R.; Castiglioni, C. *New J. Chem.* **2009**, *33*, 1542. (b) Monguzzi, A.; Trioni, M. I.; Tubino, R.; Milani, A.; Brambila, L.; Castiglioni, C. *Synth. Met.* **2009**, *159*, 2410.
(11) (a) Bischof, C.; Wahsner, J.; Scholten, J.; Trosien, S.; Seitz, M. *J. Am. Chem. Soc.* **2010**, *132*, 14334. (b) Doffek, C.; Alzakhem, N.; Molon, M.; Seitz, M. *Inorg. Chem.* **2012**, *51*, 4539. (c) Scholten, J.; Rosser, G. A.; Wahsner, J.; Alzakhem, N.; Bischof, C.; Stog, F.; Beeby, A.; Seitz, M. *J. Am. Chem. Soc.* **2012**, *134*, 13915.
(12) Lehn, J.-M.; Roth, C. O. *Helv. Chim. Acta* **1991**, *74*, 572.
(13) Crystals of [$\mathbf{D_0}$]-**Er** and [$\mathbf{D_0}$]-**Yb** were heavily disordered and extremely fragile and allowed only isotropic refinement. Nevertheless, the fundamental composition of the crystals and especially the presence of the species $[LnCl_5(H_2O)]^{2-}$ is clearly obvious.
(14) Aime, S.; Barbero, L.; Botta, M.; Ermondi, G. *J. Chem. Soc., Dalton Trans.* **1992**, 225.
(15) Peters, J. A.; Huskens, J.; Raber, D. J. *Prog. NMR Spectrosc.* **1996**, *28*, 283.
(16) Forsberg, J. H.; Delaney, R. M.; Zhao, Q.; Harakas, G.; Chandran, R. *Inorg. Chem.* **1995**, *34*, 3705.
(17) Terazzi, E.; Rivera, J.-P.; Ouali, N.; Piguet, C. *Magn. Reson. Chem.* **2006**, *44*, 539.
(18) Rodríguez-Rodríguez, A.; Esteban-Gómez, D.; de Blas, A.; Rodríguez-Blas, T.; Fekete, M.; Botta, M.; Tripier, R.; Platas-Iglesias, C. *Inorg. Chem.* **2012**, *51*, 2509.
(19) (a) Lisowski, J.; Sessler, J. L.; Lynch, V.; Mody, T. D. *J. Am. Chem. Soc.* **1995**, *117*, 2273. (b) Lima, L. M. P.; Lecointre, A.; Morfin, J.-F.; de Blas, A.; Visvikis, D.; Charbonnière, L. J.; Platas-Iglesias, C.; Tripier, R. *Inorg. Chem.* **2011**, *50*, 12508. (c) Fernández-Fernández, M.; del, C.; Bastida, R.; Macías, A.; Pérez-Lourido, P.; Platas-Iglesias, C.; Valencia, L. *Inorg. Chem.* **2006**, *45*, 4484.
(20) Beeby, A.; Burton-Pye, B. P.; Faulkner, S.; Motson, G. R.; Jeffery, J. C.; McCleverty, J. A.; Ward, M. D. *Dalton Trans.* **2002**, 1923.
(21) (a) Child, M. S.; Halonen, L. *Adv. Chem. Phys.* **1984**, *57*, 1. (b) Henry, B. R. *Acc. Chem. Res.* **1977**, *10*, 207.
(22) (a) Bini, R.; Foggi, P.; Della Valle, R. G. *J. Phys. Chem.* **1991**, *95*, 3027. (b) Kjaergaard, H. G.; Proos, R. J.; Turnbull, D. M.; Henry, B. R. *J. Phys. Chem.* **1996**, *100*, 19273. (c) Snavely, D. L.; Overly, J. A.; Walters, V. A. *Chem. Phys.* **1995**, *201*, 567.
(23) Page, R. H.; Shen, R. Y.; Lee, Y. T. *J. Chem. Phys.* **1988**, *88*, 4621.
(24) Kjaergaard, H. G.; Turnbull, D. M.; Henry, B. R. *J. Phys. Chem. A* **1997**, *101*, 2589.
(25) (a) Malta, O. L. *Phys. Lett. A* **1986**, *114*, 195. (b) Malta, O. L. *J. Non-Cryst. Solids* **2008**, *354*, 4770.